Solid-state lateral proton conduction via solid-supported biological membranes reveals the role of membrane structure and bound water in proton transport

Ambili Ramanthrikkovil Variyam,[a] Mikhail Stolov,[b] Jiajun Feng,[a] and Nadav Amdursky[a,*]

[a]Schulich Faculty of Chemistry, Technion – Israel Institute of Technology, Haifa 3200003, Israel.

[b]Wolfson Department of Chemical Engineering, Technion – Israel Institute of Technology, Haifa 3200003, Israel.

*Corresponding author email: amdursky@technion.ac.il

Keywords: Membranes, Proton transport, Lateral diffusion, Supported lipid bilayers, Proton conduction

Abstract

Lateral proton transport (PT) on the surface of biological membranes is a fundamental biochemical process in the bioenergetics of living cells, but a lack of available experimental techniques has resulted in a limited understanding of its mechanism. Here, we introduce a new molecular protonics experimental approach to investigate lateral PT across membranes by measuring long-range lateral proton conduction via a few layers of lipid bilayers in a solid-state-like environment, i.e., without having bulk water surrounding the membrane. This configuration enables focusing on lateral proton conduction across the surface of the membrane while decoupling it from bulk water. Hence, by controlling the relative humidity of the environment, we can directly explore the role of water in the lateral PT process. We show that proton conduction is dependent on the amount of water and their structure, and on membrane composition, where we explore the role of the head group, the level of tail saturation, and the role of the membrane phase and fluidity. The measured PT as a function of temperature shows an inverse temperature dependency, which we explain by the desorption/adsorption of water molecules into the solid membrane platform. We explain our findings by discussing the role of percolating hydrogen bonding within the membrane structure in a Grotthuss-like mechanism.

Introduction

Proton transport (PT) circuits involving biological membranes are of prime importance and they are in the heart of our aerobic respiration system and of plants' photosystem. When we discuss PT in the context of biological membranes, we need to differentiate between proton translocation across the two sides of the membrane, which is assisted by transmembrane protein, to lateral proton diffusion on the surface of the membrane. Such lateral PT along membranes and its interface with the bulk aqueous environment have been identified and distinguished from PT in water more than 25 years ago,[1-4] and an apparent barrier exists across the bulk water-membrane interface, which affects proton activity at this interface.[3, 5-19] Several experimental works have shown the capability to observe long-range PT on the surface of biological membranes and that the membrane composition can have an effect on this lateral PT.[7, 20-25] However, to date, most studies concerning long-range lateral PT (diffusion) on the surface of membranes were of spectroscopical nature and consisted of a molecular proton donor/acceptor situated at a certain position in the system. Here, we are introducing the first in-depth exploration of the ability of membranes to support long-range lateral PT using electrical measurements, i.e., following proton conduction in a solid-state type of molecular protonics device.

The electrical properties of membranes have been investigated for many decades, already from the late 1960s, following the discovery of the first model system that mimics the plasma membrane called black lipid membranes, for which the degree of ion impermeability across the lipid bilayers was evaluated in terms of ohmic resistance (in the order of a few MΩ·cm).[26-28] During the 1980s, an additional membrane model was introduced, which is the supported lipid bilayer (SLB).[29] Due to the planar structure and compatibility with surface-based analytical methods, SLBs have become a platform for understanding the structure and physical characteristics of cell membranes[30-32] and in biosensor applications.[33-35] SLBs have also been characterized by electrical measurements across them, many utilizing impedance spectroscopy, particularly in understanding the interaction between membrane surfaces and their surroundings.[36-39] In this context, we should also mention the widely used patch-clamp technique to follow the electrical resistance of biological membranes.[40-42] Importantly, no

matter the chosen membrane model, the electrical measurements targeted the electrical response across the two sides of the membrane, i.e., through its nm-scale thickness and not its lateral parameters, and were performed with bulk water either on one side of the membrane (with SLB) or on both sides.

In this work, we introduce a new methodology to probe long-range lateral PT on the surface of biological membranes. As stated, our methodology is based on following lateral proton conduction in a solid-state-like environment using molecular protonics devices composed of nm-scaled SLBs, meaning a solid sample in an environment with a certain relative humidity (RH). The solid-state environment enables focusing directly on the role of the membrane surface and its composition in supporting lateral proton conduction while decoupling it from surface to bulk (or *vice versa*) events of PT. Thus, we can estimate the number of water molecules on the surface of the membrane, the water structure, and explore the role of water molecules within the membrane structure in supporting this long-range lateral proton conduction. Our temperature-dependence measurements of proton conductance show an interesting inverse temperature dependency, i.e., the conductance decreases as a function of temperature. We ascribe this peculiar finding to the number of water molecules on the surface of the membrane, which is yet another indication of the role of water molecules in assisting lateral PT across the membrane. We discuss the possible proton conduction mechanism at different membrane conditions, where we show the importance of several lipid parameters: headgroup, tail, phase, and fluidity, in supporting protonic conduction due to its ability to form a percolating hydrogen bond network. In addition to our new fundamental understanding of long-range PT on the surface of biological membranes, our findings of the specific role of the membrane interface in supporting lateral long-range PT is important to any use of membranes in various applications, from biomedical applications to the use of proton-conductive membranes in energy-related applications.

Results

Making and characterizing the supported lipid bilayers in the solid-state

SLBs are generally prepared using Langmuir – Blodgett film transfer or via vesicle fusion. These approaches produce a bilayer membrane on top of a hydrophilic surface like Si oxide (SiO_x) or glass in an aqueous environment.[43-45] The presence of the aqueous environment is mandatory for the SLB configuration as it will collapse in a solid-state environment. As we aim here to probe the lateral proton conduction in a molecular protonics solid-state device, we need to remove the aqueous phase from the system. To do so, we used spin-coating of a lipid solution on top of a SiO_x wafer, which resulted in a thin film of lipid bilayers (Figure 1). To understand how many SLBs we have in our sample, we turned to various characterization techniques: Ellipsometry, atomic force microscopy (AFM), and X-ray reflectivity (XRR). Both ellipsometry and XRR are reflection-based techniques to characterize thin films. Ellipsometry measures changes in the visible light polarization upon interaction with a material, which is commonly translated to the thickness of the dielectric layer. In our ellipsometer measurements, we have estimated the thickness of the spin-coated SLBs to be ~20 nm regardless of the lipid used to form the structure. XRR is more sensitive to the internal ordering of the thin film. Our XRR measurements (Figure S1 and text within) clearly show a repeating structure within the thin film that can be modeled to ~4-5 bilayers of membranes. To complement these measurements, we turned to AFM which can both estimate the thickness of the film as well as its uniformity. In Figure 1, we show an AFM image of the edges of the spin-coated area that allows us to observe the individual layers within our multi-SLB. In line with our ellipsometer measurements, also the AFM images confirm that the thickness of the film is ~20 nm. Thus, all indications point to a thin film of SLBs composed of 4-5 membrane bilayers with a height of ~20 nm. It is very important to note in this stage that all lipids used in this study (Table S1) have resulted in similar multi-SLB films with similar thicknesses. Nevertheless, it is also important to mention that due to the deposition technique of the multi-SLB using spin coating for a macroscopic surface area, we found some variance in the uniformity of the film in different areas of the macroscopic surface (Figure S2). As can be observed in Figure S2, whereas some areas are highly uniform, other areas contain patches within the surface, whereas all the different lipids used in this study resulted in a similar pattern in the AFM measurements. The long-range proton conductance measurement averages the whole surface.

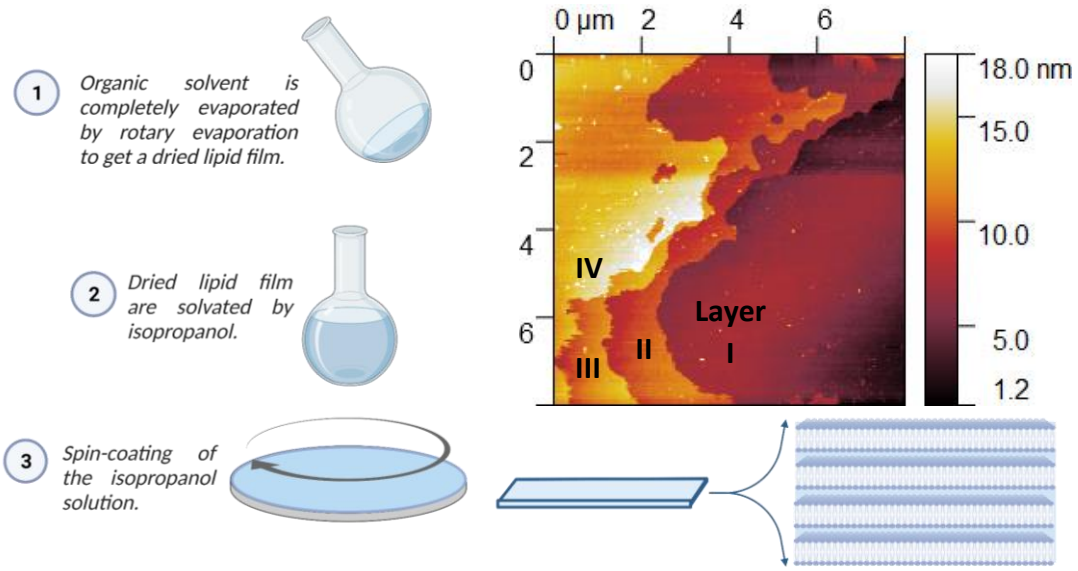

Figure 1. General procedure of solid state SLBs preparation by spin coating of lipid solutions (left) and the AFM image of SLBs (DLPC lipid in this case, Table S1 for the chemical name and structure) prepared on a SiO_x surface showing four layers of membranes (right).

Lateral proton conduction across the supported lipid bilayers in the solid-state

Following validating the making of the multi-SLB films, we prepared them on an array of interdigitated metal electrodes made by Pd (for reasons that will be discussed below) on a SiO_x surface with a distance between electrodes of 70 µm. We measured the long-range conductance of the electrical device using both ac-bias-driven electrochemical impedance spectroscopy (EIS) and dc-bias-driven current-voltage (I-V) measurements. The importance of EIS measurements for estimating bulk resistance properties of layers is due to their ability to decouple bulk charge resistance which is the prominent process at high ac frequencies to any processes happening next to the surface of the electrodes that are prominent at low ac frequencies. Accordingly, to calculate the conductivity values of all lipids used in this study, we have used the EIS result and fitted them to an equivalent circuit (Figure S4 and text within). It is worth mentioning that the conductivity extracted from a Pd-based device is similar to the one extracted from multi-SLB films on the more common Au-based device (Figure S3 and discussed in Ref.[46]). It is important to note that an EIS or I-V measurement by itself is not enough to conclude the nature of the charge carrier. However, we can already safely assume that proton conduction is the most likely source of the measured conductance as any electronic conduction is very unlikely for such distances using an electronic-insulator type of materials

as membranes and any other ionic transport is also unlikely as we did not introduce any ions to the system. Nonetheless, we introduce here two important experiments to determine the protonic conductance nature of our measurements. The first experiment is a RH-dependency of the EIS measurements (Figure 2a, shown as a Nyquist plot representation - imaginary part of impedance vs the real part, whereas the plots of all lipids are shown in Figure S5). In general, all 'soft' proton conductors should exhibit a RH-dependency of their proton conductance, as water molecules are essential in supporting proton conduction through a percolating hydrogen bonds network (further discussion below). As clearly seen in Figure 2a, the impedance resistance is reducing as a function of RH, thus validating the role of protons as charge carriers across the membrane sample. The I-V measurements further show RH-dependency (Figure S6), but with smaller amplitude due to the discussed differences between these methodologies. The second important experiment to prove PT is performing I-V measurements with the Pd electrodes before and after their hydrogenation to PdH_x (Figure 2b). PdH_x electrodes are known for their capability to perform as proton transparent electrodes, meaning they can inject protons directly into the sample as opposed to the common electronic injection of metal electrodes.[47-50] As shown in Figure 2b, the I-V measurements show a vast increase in measured current following the formation of the PdH_x electrodes, which is an indication of a proton-conductive material. The hysteresis in the I-V measurements is due to the double-layer capacitive nature, resulting from the presence of water molecules in our system.

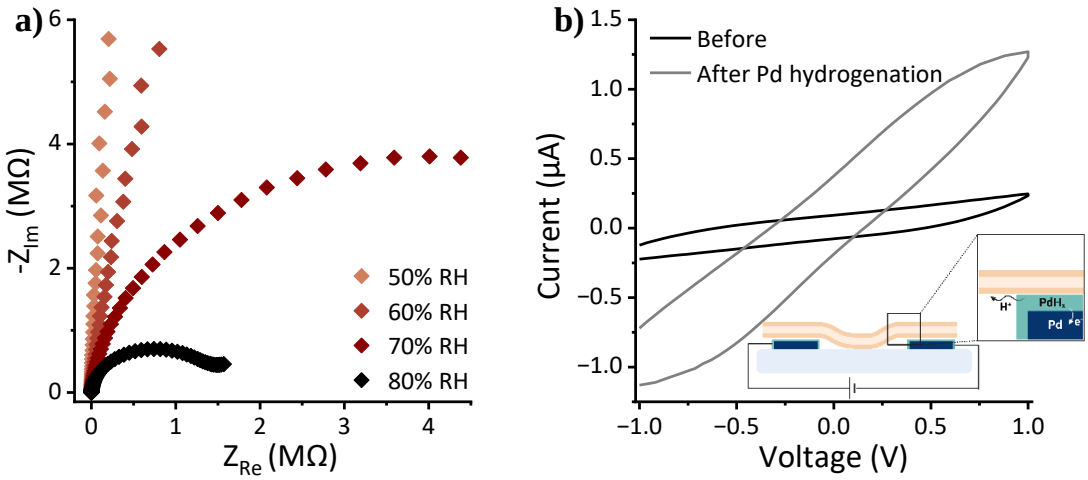

Figure 2. (a) EIS measurements of a device with a multi-SLB film at different relative humidities. (b) I-V measurements of a multi-SLB film before and after the formation of the hydrogenated Pd electrode. The inset shows a schematic of the PdH_x setup. Both panels show

the results with DMPA SLBs (Table S1 for the chemical name and structure), whereas the RH-dependent EIS and I-V measurements of all other SLBs films explored here are presented in Figure S5 and S6, respectively.

The role of membrane parameters in dictating proton conduction

After confirming that protonic conduction is what we measure in our molecular protonic devices, we turned to decipher the role of different parameters associated with the membrane properties on the protonic conductivity of the multi-SLB film. Figure 3 summarizes the conductivity values of all lipids investigated here. The figure shows the measured protonic conductivity at 80% RH (at room temperature (RT), ~23°C) as it is the highest measured conductivity, but, very importantly, the below discussed trends are identical for all the different RH values (Table S2 for the conductivity values in different RH values probed). We can differentiate between the different lipids in terms of three important structural motifs:

1) Head groups (Figure 3a): In accordance with our hypothesis, and in line with previous studies, the head group of a lipid should be a crucial component in the ability of the multi-SLB to support protonic conduction because of the capability of both the phosphate group and the charged/polar headgroup to participate in a hydrogen bond network. Here, we examine four distinct groups: phosphatic acid (PA), phosphatidyl glycerol (PG), phosphatidylcholine (PC), and phosphatidyl ethanolamine (PE) where the first two are negatively charged and the latter two are zwitterionic (see schematic in Figure 3a and Table S1). Importantly, for a fair comparison, all the different lipids in this section shared the same unsaturated tale. From the impedance experiments and the extracted conductivity values, we can rank the conductivity values of the different as follows: PG>PC>PE>PA ($3.00\pm0.36 > 2.26\pm0.15 > 1.12\pm0.04 > 0.32\pm0.06$ $mS\cdot cm^{-1}$, respectively). Our results clearly point out the fundamental role of the head group in supporting long-range lateral proton conduction in the solid-state-like environment. Interestingly, the PA-terminated lipid is notably less proton conductive than the other bulkier lipids, highlighting the role of chemically 'shielding' the phosphate group in the PT mechanism, which will be discussed below.

2) The melting point of lipids - Number of carbon atoms in the tail part (Figure 3b): For saturated lipids, the number of carbon atoms on the tail is directly related to the melting point. In this section, we compared the protonic conductivity across membranes composed of lipids with PC head groups but differentiated by the number of saturated carbons in their tails: DLPC (12C), DMPC (14C), and DPPC (16C) with melting points of -2°C, 23°C, and 44°C, respectively. As we measure at RT, DLPC is in its liquid state, DMPC is semi-liquid, i.e., in the transition from liquid to gel, and DPPC is in its gel phase. Our results clearly show that a membrane in its liquid state is more conductive than a membrane in its gel phase. However, are all membranes in the same phase and with the same headgroup have a similar proton conductance? A question that leads us to the next point.
3) Saturate vs. unsaturation tail groups (Figure 3c): The level of saturation of lipids tails can have a vast effect on various membrane properties, primarily, the fluidity of the membrane. For a fair comparison in this section, we compared two membranes with an identical melting point and a similar headgroup, where we chose POPC (unsaturated) and DLPC (saturated) having a melting point of -2˚C (Table S1), thus, they are liquid in RT. Our results indicate that the saturated membrane is more conductive than the unsaturated one. Importantly, our conclusion here that saturated membranes are more proton conductive than unsaturated membranes is also valid by comparing the saturated DMPA to the unsaturated POPA and the saturated DMPG to the unsaturated POPG. Albeit in these examples, the membranes do not share an identical melting point, but they are in the same phase in RT. Our observation that membranes composed of saturated lipids are more conductive than membranes composed of unsaturated lipids is counter intuitive since membranes of unsaturated lipids are more fluid than membranes of saturated lipids, and as observed in the previous discussion, fluid liquid membranes are more conductive than gel membranes. Accordingly, this observation hints that there might be another parameter involve in proton conduction here, which leads us to the next discussion about the role of water molecules.

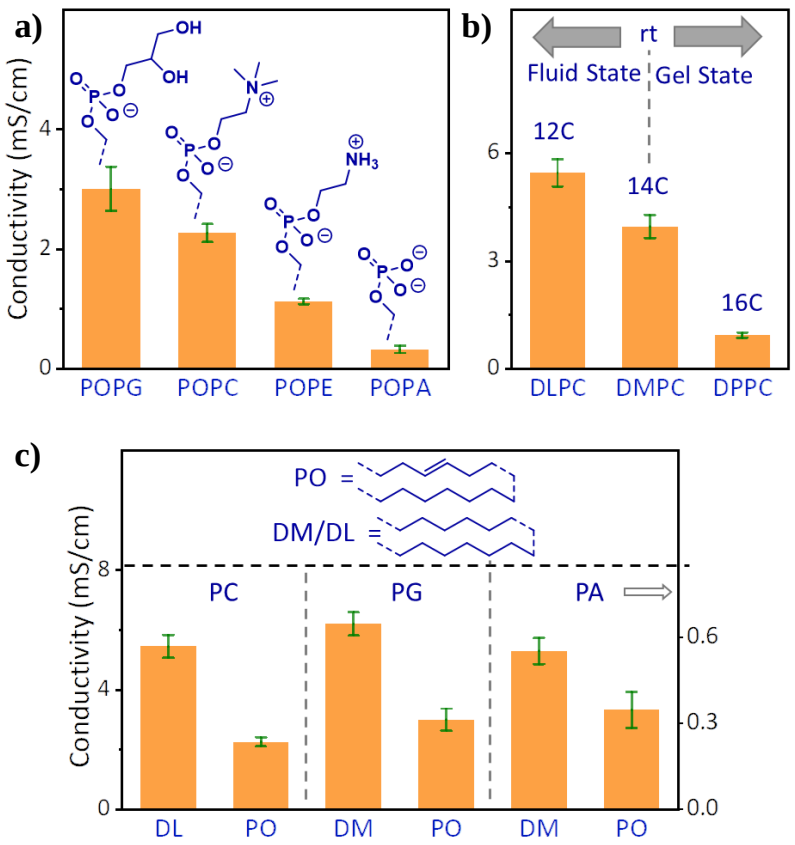

Figure 3. The conductivity at RT and 80% RH of all the different multi-SLB films under investigation as a function of: (a) Head group; (b) Melting point/number of tail carbon atoms; (c) Tail saturation (the conductivity values of 'PA' are on the right y-axis). The error bars represent standard deviation of N>3 samples for each studied membrane.

The role of water in proton conduction

In this section, we characterize the hydration of each multi-SLB; the amount of water molecules adsorbed to the multi-SLB structure following its formation, as well as the structure of the water molecules network within the membrane. Because of the solid-state nature of the multi-SLB structure, the amount of water molecules can be measured by weighing the final structure (see experimental section). Figure 4 shows the calculated number of water molecules per lipid molecule in each of the membranes measured in the conductivity measurements (as in Figure 3). When we compared the water content for membranes of lipids having the same unsaturated tail but different headgroups, we observed a similar water content (Figure 4a). Similarly, when we compared the water content for membranes of lipids with the same headgroup but different saturated tails, we also observed a similar water content (Figure 4b). These observations indicate that the change in proton conductivity measured in Figure 3a and 3b can be ascribed

to the nature of the headgroup and the membrane phase, respectively. However, when we compared the water content for membranes of saturated vs. unsaturated lipids, having the same headgroup, we found a large change in water content, whereas membranes of saturated lipids have more water content than unsaturated lipids (Figure 4c). As will be discussed below, this important observation is the most likely explanation for the change in conductivity observed in Figure 3c.

Another important parameter of the water within the multi-SLB construct is related to the structure of the water molecules' network within the membrane, which is an important factor in the ability of the material to transport protons in a Grotthuss-like mechanism (*vide infra*). To this end, we used FTIR, which is an important tool in discerning the hydration properties of lipid membranes.[51-57] One of the prominent bands in the FTIR of hydrated lipid membranes is the classic O-H stretching band of water molecules centered at 3400 cm^{-1}, which is sensitive to the extent of H-bonding in the film.[51] Our FTIR measurements of the membranes in their multi-SLB configuration show that there are two main FTIR peaks in this region, and different membranes having different contributions from these two peaks (Figure 4d and Figure S7). These peaks are at 3400 and 3250 cm^{-1}, whereas the former represents the classic O-H stretching band of water, while the latter attributes to O-H stretching of water molecules in a large network of H-bonded structure.[51, 54] Accordingly, the ratio between these peaks is indicative whether most of the water molecules are within a large network of H-bonded structure, thus exhibiting a predominant 3250 cm^{-1} peak, or they are not part of a network, thus exhibiting a predominant 3400 cm^{-1} peak. While comparing the FTIR spectra of the multi-SLB composed of POPG, POPC, POPE, and POPA, i.e., having the same tail at the same membrane phase but differentiated in their headgroup, we can clearly see a different FTIR pattern (Figure 4d). Membranes of POPG exhibit only the 3250 cm^{-1} peak, thus indicating that the water molecules within them are mostly networked, whereas membranes of POPA exhibit only the 3400 cm^{-1} peak, thus indicating that the water molecules within them are mostly not networked. Membranes of POPC and POPE show both peaks. Since we found that membranes of POPG are the most conductive and the ones of POPA are the least conductive (Figure 3a), the observation in this part points on the role of networked water in the ability of the membrane to

be conductive. We further found that all PC-terminated membranes have the discussed two FTIR peaks, PA-terminated membranes have only the 3400 cm^{-1} peak, and PG-terminated membranes have only the 3250 cm^{-1} peak (Figure S7), but it is more complicated to compare the FTIR measurements for membranes having different phases or fluidity.

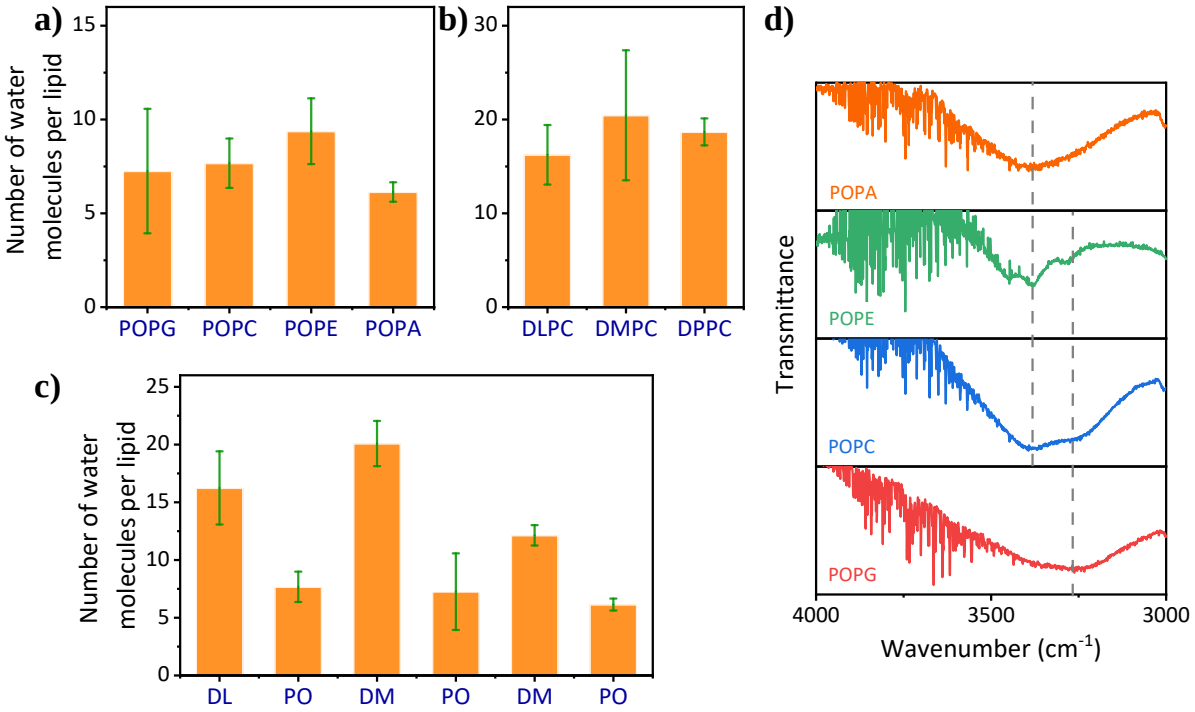

Figure 4: Results from the calculation of number of water molecules per lipid at RT and 60% RH for all the lipid films as a function of (a) Headgroup; (b) Melting point/ number of carbon atoms on tail and (c) Tail saturation. (d) FTIR diagrams of lipid films as a function of their headgroup at RT and 60% RH showing vibrational bands between 3000-4000 cm^{-1}. N>3 for the number of samples for each studied membrane.

The effect of temperature on proton conduction

In general, proton conduction, no matter the mechanism, should be a thermally-activated process, meaning the conductance should go up with temperature. To our surprise, we observed an inverse temperature dependency in both our impedance (Figure 5a and Figure S8 for all lipids) and I-V (Figure 5b and Figure S9 for all lipids) measurements, i.e., the measured conductance/current was decreasing as a function of temperature. The temperature range that we used is 15°C to 35°C to avoid condensation of water molecules that started to appear below the range, while above this temperature range, the conductivity reached a very small value.

Importantly, this inverse temperature dependence is reversible for several cycles of heating-cooling (Figure 5b and Figure S10). While plotting the dependency of the extracted protonic conductivity from the EIS measurements as a function of temperature (Figure S11 for all the lipids), we can see a trend for the decrease of extracted conductivity with temperature. Specifically, for DMPG and DMPC, we have extended our temperature range to have the melting point temperature of these SLBs (~23-24˚C) in the middle of the measured temperature range, thus allowing us to explore the role of the membrane phase in the temperature dependency of proton conduction. We can clearly see that the different membrane phases, i.e., liquid vs. gel phases, have a different dependency with temperature (Figure 5c, green and orange areas, respectively). Importantly, the dependency of the conduction with temperature is around 2-fold larger for the gel phase than for the liquid phase, meaning that for the gel phase, a small temperature change is resulting in a larger change in conductivity than in the liquid phase. It is also important to note that the changes in the conductivity for the different lipid characteristics as presented in Figure 3 remains similar at different temperatures (Table S3).

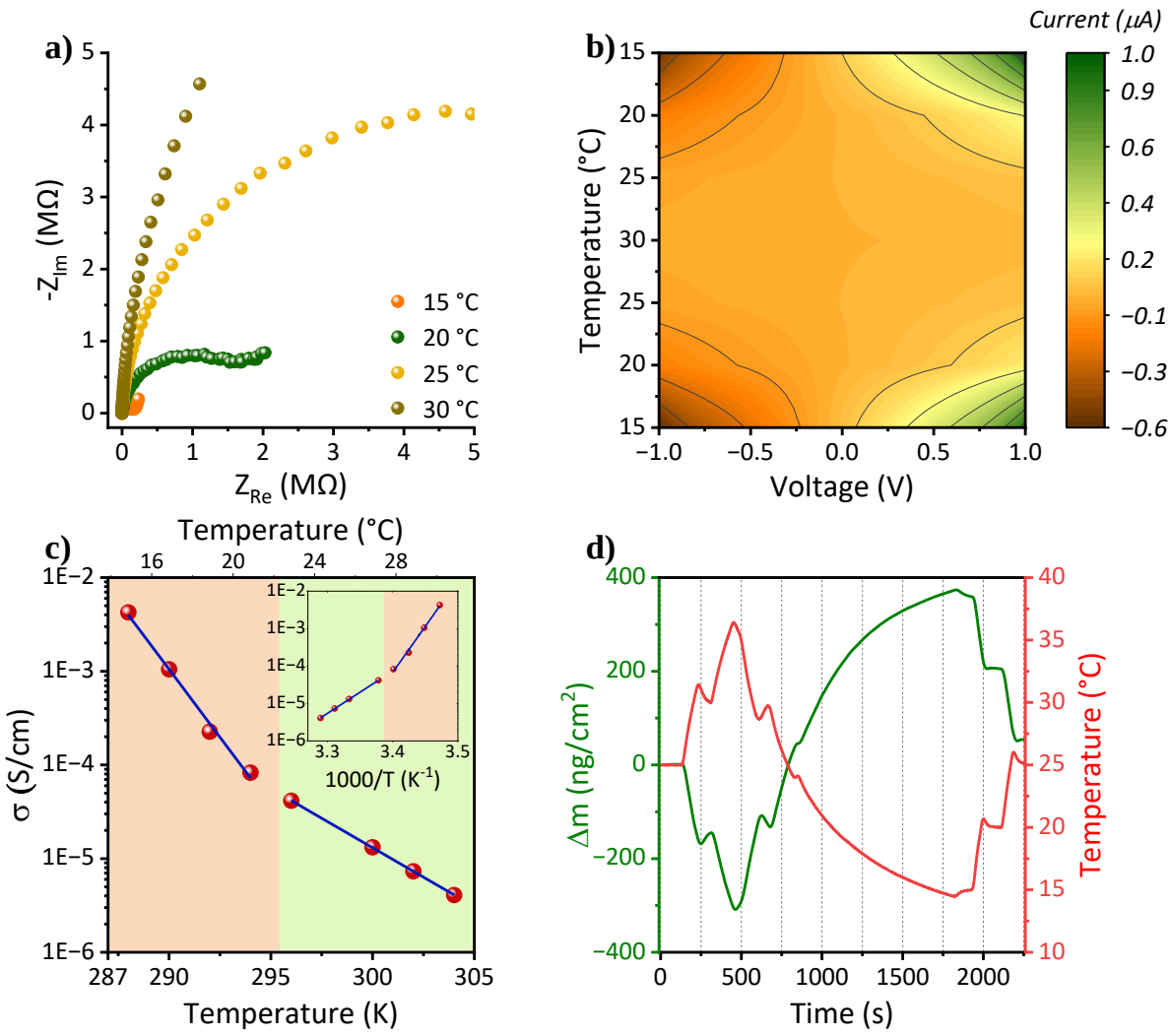

Figure 5. Temperature-dependent electrical measurements of a SLB films using (a) impedance measurements and (b) I-V measurements. The graph in panel (b) shows the reversibility of protonic currents on heating and cooling cycle, while the current is displayed as a heatmap. The panels (a) and (b) show the results for the POPC multi-SLB film, whereas the EIS and I-Vs measurements for all lipids are displayed in Figures S8 and S9, respectively. (c) The extracted conductivity as a function of temperature for the DMPG multi-SLB film covering the range of the two membrane phases, gel and liquid, marked with orange and green rectangles, respectively. Similar graphs for all other SLBs films are presented in Figure S11. The inset shows the same on a 1000/T x-axis. (d) QCM measurement of a DMPG multi-SLB film upon one cycle of heating and cooling (Figure S12 shows multiple cycles).

To rationalize the inverse temperature dependency of protonic conduction, we have conducted several types of experiments. First, we have used temperature dependence XRR measurements to follow any noticeable changes in the thickness of the SLBs film or its internal structure. As shown in Figure S13, we observed no change in the XRR pattern at different temperatures, thus

indicating that the observed inverse temperature dependence of the measured protonic conduction is not due to a change in the membrane structure within the SLB configuration.

Since water molecules have an important role in the ability to support long-range proton conduction by assisting in forming hydrogen bond networks, the next immediate suspect to rationale the inverse temperature dependence is the number of water molecules in the SLBs film. For that matter, we used temperature-dependence quartz crystal microbalance (QCM) measurements to estimate the change in mass of the films at different temperatures. We detected a reversible mass change of the film as a function of temperature, where increasing the temperature resulted in a decrease in mass (Figure 5d) and vice-versa for numerous cycles (Figure S12). In our QCM measurements, we can safely conclude that the observed change in mass is due to water molecules. Thus, highlighting the role of water molecules in supporting the observed proton conduction in a mechanism that will be described below.

Does proton conduction happen across the entire cross-section of the multi-SLB film or not?

To answer this question, in the last part of our proton conduction measurements, we investigated the role of film thickness and its temperature dependency on the measured proton conductivity. In accordance with our new methodology, the thickness of the multi-SLB film can be easily tuned by varying the rpm and time of the spin-coating process (the 20 nm multi-SLB film discussed thus far represents the minimum thickness). Thickness-dependent measurements can resolve if the conductance is happening through the entire cross-section of the membrane or just next to the bottom surface, which is in contact with the electrodes in its edges. As shown in Figure S14, the measured conductance is increasing as a function of thickness, but the measured conductivity is similar regardless of the thickness. Thus, implying that the measured protonic transport is happening through the entire cross-section of the film and that all the bilayers in the multi-SLB structure contribute to the measured proton conductance. Nevertheless, the temperature dependency is different between different thicknesses, whereas the thicker the film the (inverse) temperature dependency is smaller, as observed both in the EIS measurements (Figure 6a-6b) and in the I-V measurements (Figure 6c-6d). To explain this result, we have compared the temperature dependence QCM measurement between the thin and the thick sample (Figure 6e-6f), where we observed a

relative similar order of change in mass between the sample (even smaller changes in the thick sample). This indicates that the amount of water loss/gain per mass of lipid is much smaller in the thick sample than the thin one, which is translated to a much smaller change in the conductance as a function of temperature.

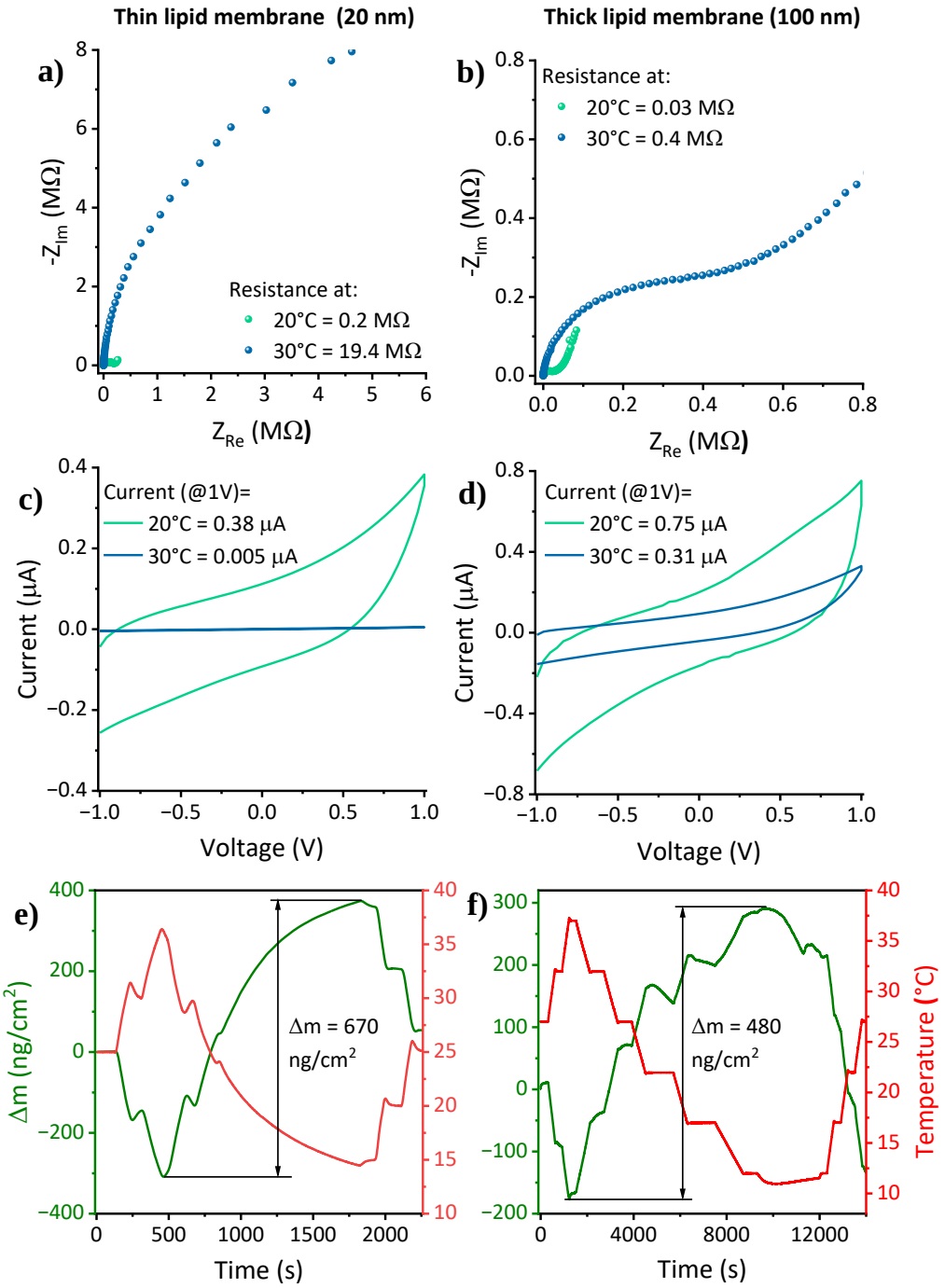

Figure 6. (a) and (b) Impedance measurements and (c) and (d) I-V measurements of a thin (20 nm) SLBs film ((a) and (c)) and a thick (100 nm) SLBs film ((b) and (d)) at two different temperatures. (e) and (f) Temperature-dependence QCM measurements of the thin and thick SLBs films, respectively. All measurements here were conducted with DMPG SLBs.

Discussion

In the discussion part, we intend to detail our suggested PT mechanism across the multi-SLB films composed of different lipids that can explain our presented results. At first, we need to discuss the conventional PT mechanism across soft biological materials in a solid-state-like environment. We define such an environment as having a solid sample that contains a certain amount of water and the environment is at a certain RH. To date, most of the reported soft biological materials that are showing protonic conductivity in these solid-state conditions are either composed of proteins (or peptides) or polysaccharides.[47-50, 58-66] In terms of measured conductivity, most of the multi-SLB films used in this study are in the upper end of reported conductivity values for proteins and polysaccharides. The common long-range PT mechanism suggested for all the solid-state biological materials is the Grotthuss mechanism. This mechanism is based on proton hopping along a hydrogen bond network. It was shown in several studies that in solid-state biological materials, this network is composed of both water molecules within the material and specific polar or charged moieties of the biological entity, which are the amino acid residues in proteins or the polar groups in glycan chains.[48, 59, 61, 64-68] Accordingly, the hydrogen bond network is facilitated within the interface of the biological material and the trapped water molecules bound to it. It is important to note also that this mechanism is similar to the common convention of hydrogen bond networks within natural proteins capable of proton translocation, such as the transmembrane proteins in photosynthesis or the aerobic respiration system. In addition to the Grotthuss mechanism, the main other suggested mechanism for soft matter in the solid-state is the vehicular mechanism, which is the movement of ions (as hydronium) via a vehicle that is usually water molecules surrounding the ion. To facilitate this type of mechanism there is a need for large water cavities within the material, which is not the case in the multi-SLB film. Hence, in line with all other biological materials, the Grotthuss mechanism is the suggested mechanism also in our case.

Now, to discuss the specific hydrogen bond network responsible for the measured proton conduction we will refer to our measurements with different lipid headgroups (Figure 3a). In these measurements, we observed that PT across PA-terminated SLBs is significantly poorer than the other lipids used. This is somewhat in contrast to measurements done with single lipid

bilayers in solution (in a form of a vesicle), where it was shown that PA lipids can facilitate PT via interactions of surface-to-bulk or bulk-to-surface.[22, 25] In our case, we do not have a bulk solution, hence there are no such interactions. On the contrary, our observation that the additional chemical moieties, regardless of them being charged or not, on top of the phosphate group are resulting in an increase in PT compared to the bare PA points on a 'shielding' effect of them. Accordingly, the only rationale mechanism to explain it is the presence of a hydrogen bond network of trapped water molecules and the phosphate backbone of the lipids for the formation of shielded network wires. In that sense, a polar moiety (PG-terminated) is more efficient in the formation of the hydrogen bond network than a positively charged group (PC-terminated), and a bulkier group (PC) is more efficient than a less bulky group (PE-terminated, which is also positively charged). Our FTIR measurements (Figure 4d) highly support this explanation by showing that water molecules within PG-terminated membranes are in a network configuration, while in PA-terminated membranes they are not. In this context, it is important to mention earlier works that discussed the importance of water wires in the ability to facilitate PT in high efficiencies, either within proteins or even on the surface of the membrane.[69-74]

In terms of temperature dependency, the Grotthuss mechanism should be thermally activated with a commonly measured activation energy in the order of 0.1-0.2 eV.[69] However, we observed an inverse temperature dependency. To explain this, we should realize that our multi-SLB films contain a low amount of water, and as such, a small amount of water loss can have a huge effect on the intactness of the hydrogen bond network, which will result in a poor PT across the material (as observed). In our case, heating is inducing the desorption of water molecules while cooling is resulting in their re-absorption from the humid environment. Our results of a less drastic inverse temperature dependency of the thicker SLBs films support this hypothesis.

The last point in the mechanism discussion is related to the effect of the membrane phase and membrane fluidity on the PT properties. Here, we observed two important observations. 1) PT across a gel phase of the membrane is less efficient than across its liquid phase (Figure 3b). Here, we can safely claim that there is a need for membrane flexibility, which is present only

in the membrane liquid phase, to facilitate the formation of a percolating hydrogen bond network within the discussed shielded wire composed of phosphate backbones. Our observation of a different thermal response of measured conductivity at the different phases of a certain membrane supports this notion (Figure 5c). 2) PT across a more fluid membrane composed of un-saturated lipids is less efficient than across a less fluid membrane composed of saturated lipids having the same headgroup (Figure 3c). This observation is counterintuitive as we would expect that a more fluid membrane will have better PT capabilities than a less fluid one. On the other side, we observed a different water content for these two membrane compositions, whereas saturated lipids contain more water in the multi-SLB configuration than un-saturated lipids. Accordingly, the changes in the PT efficiency here should be explained in terms of the amount of water molecules, i.e., more water molecules, a better network of hydrogen bonds.

Overall, all experimental indications point to a sweet point for the most efficient PT across the solid membrane films: We want the membrane to be in its liquid state with high water content and with a bulky polar headgroup. This is the reason why the saturated DMPG membrane with a melting point below RT is the most conductive film in our study.

Conclusions

In summary, we have designed and created a novel model of multi-SLB film that is composed of 4-5 bilayers of membranes in a solid-state-like environment to investigate the lateral proton conduction for long distances across the membranes in a molecular protonics device. Proton conduction was confirmed by both RH-dependent measurement and the use of proton transparent electrodes. In terms of how the composition of the membrane affects the measured protonic conductivity, we found that: 1) the lipid head group is of prime importance with the following trend in proton conductivity: PG>PC>PE>PA; 2) the lipid phase influence the measured conductivity, whereas fluid membranes conduct better than gel membranes; 3) membrane of saturated lipid conduct better than unsaturated lipids even though membranes of unsaturated lipids are more fluid than saturated ones. By measuring the water content and the water structure within the multi-SLB configuration, we could rationale why membranes of

unsaturated lipids are poorer proton mediators compared to membranes of saturated lipids. We show that the most conductive PG-terminated membrane is having water molecules in a network structure, while the least conductive PA-terminated membrane does not have such a network. In terms of how temperature affects the measured proton conductivity, we found an inverse temperature dependency for all investigated membranes. QCM measurements has resulted in our understanding that the desorption/adsorption of water molecules from the multi-SLB film is the main factor responsible for the observed inverse temperature dependency. In terms of the PT mechanism, we discussed how the Grotthuss mechanism can be applied to our results and how the change in the different parameters can influence the percolating hydrogen bond network across the membrane surface that is needed for an efficient PT.

Materials and Methods

Sample preparation: Each lipid was dissolved in chloroform followed by solvent evaporation using a rotary evaporator until a dried lipid film was formed. The lipid film was kept overnight inside the vacuum chamber and was redissolved in isopropanol to a lipid concentration of 3 mg/ml.

Electrode preparation: The devices were prepared using silicon wafers with SiO_x dielectric layer (110 nm). 200 nm Au/Pd electrodes were deposited on 40 nm Cr on top of the substrates through a shadow mask using a thermal evaporator at a deposition rate of 2 Å s^{-1} under 5 × 10^{-7} Torr for the making of interdigitated electrodes (distance between electrodes of 70 μm).

Spin coating: 100 μl of the lipid-containing isopropanol solution was added on a silicon wafer and spin-coated at a rate of 2000 rpm for 120 seconds using a spin coater (EZ – spin A1, Apex instruments).

Electrochemical impedance spectroscopy: Proton conductivity measurements were carried out using an impedance/gain-phase analyzer (MTZ-35, Bio-Logic). Lipid samples were spin-coated on the prepared electrodes. The electrodes were made to be in contact using a probe station micromanipulator. A 50 mV AC bias was applied during the measurements and a frequency range of 10 MHz to 10 Hz was used for the experiments. Temperature-dependent

studies were performed using a Peltier-containing probe station (INSTEC) in the range of 15 °C to 35 °C. The conductivity of the films was calculated using the following equation: G = σA/l, where G is the conductance (as extracted using the equivalent circuit), σ is the conductivity, A is the cross-sectional area of the lipid film (A = thickness of film × width of the film), and l is the distance between two electrodes. For each condition, more than three different samples have been measured for calculating the standard deviation of the results.

Current–voltage measurements: Current–voltage measurements (I–V) were carried out using a source-measuring unit (B2912A, Agilent). Lipid films were placed on top of the Au/Pd electrodes for the I–V measurements. The current was measured as a function of voltage between -1 V and 1 V, at a scan rate of 100 mV s^{-1}. Hydrogen gas was supplied into the probe station for approximately 30 minutes to create hydrogenated Pd electrodes. The temperature-dependent studies were conducted as above mentioned.

Atomic force microscopy: The AFM measurements (XE-100 AFM, Park Systems) were performed in a tapping mode using NSG30 AFM probes (spring constant of ~40 N/m) below the resonant frequency (typically, 320 kHz) under ambient conditions at room temperature. The resulting images were processed using Gwyddion software.

Ellipsometry: Ellipsometry experiments (ALPHA-SE ellipsometer, J.A. Woollam Co.) were carried out at an incident angle of 70° with respect to the surface normal.

Fourier-transform infrared (FTIR) spectroscopy: FTIR measurements (Tensor 27 spectrometer, Bruker) were acquired in the range of 400 to 4000 cm^{-1}. For each sample, background was measured and subtracted from the spectrum. The samples were prepared using drop casting of lipid solution on a silicone surface.

Number of water molecules per lipid: Thick multi-SLB films were formed as described above on SiO_x. The mass of each lipid film was measured using a microbalance to calculate the amount of water associated with each of the films at RT and 60% RH.

X-ray reflectometry: The XRR measurements were carried out using the X-ray reflectivity mode of the Rikagu SmartLab high-resolution diffraction system.

Quartz crystal microbalance: Before the experiment, gold-plated QCM sensors (Renlux Crystal, 5.0 MHz resonant frequency) were prepared as described previously.[75] Sensors were first cleaned in a UV-ozone chamber (ProCleaner, BioForce Nanosciences) for 15 min, sonicated in 98% ethanol for 15 min, rinsed in ultrapure water for 3 min, dried by nitrogen, and cleaned again in UV-ozone for 15 min. Frequency shifts Δf were recorded for the 3rd, 5th, 7th, 9th, 11th, and 13th overtones using a Q-Sense E4 (Biolin Scientific) module. Δf was recorded in the air for the blank and coated sensor to estimate the attached film mass using the Sauerbrey equation.[76] The experiment was conducted at two humidity regimes: dry nitrogen, or nitrogen, saturated with water vapor. The flow of appropriate gas was purged through the series of two QCM cells with coated and reference sensors at 100 µl/min rate using IsmaTec peristaltic pump (IDEX) both during the measurement and for at least three hours beforehand for equilibration. During the measurement, the temperature was varied according to the programmed loop. The change in the sample mass was calculated using the Sauerbrey equation.

Acknowledgment

The authors thank Y. Zimmerman for assisting with AFM measurements and Dr. M. Koifman and A. Twersky for assisting with XRR measurements. N.A. thanks the Binational Science Foundation (grant number 2018239) and the Lower Saxony – Israel Research Cooperation (grant number ZN3625) for financial support.

References

1. Alexiev, U.; Mollaaghababa, R.; Scherrer, P.; Khorana, H. G.; Heyn, M. P., Rapid long-range proton diffusion along the surface of the purple membrane and delayed proton transfer into the bulk. *Proc. Natl. Acad. Sci. U.S.A.* **1995,** *92* (2), 372-376.
2. Gopta, O. A.; Cherepanov, D. A.; Junge, W.; Mulkidjanian, A. Y., Proton transfer from the bulk to the bound ubiquinone Q(B) of the reaction center in chromatophores of Rhodobacter sphaeroides: Retarded conveyance by neutral water. *Proc. Natl. Acad. Sci. U.S.A.* **1999,** *96* (23), 13159-13164.
3. Heberle, J.; Riesle, J.; Thiedemann, G.; Oesterhelt, D.; Dencher, N. A., Proton migration along the membrane-surface and retarded surface to bulk transfer *Nature* **1994,** *370* (6488), 379-382.

4. Teissie, J.; Prats, M.; Soucaille, P.; Tocanne, J. F., Evidence for conduction of protons along the interface between water and a polar lipid monolayer. *Proc. Natl. Acad. Sci. U.S.A.* **1985,** *82* (10), 3217-3221.

5. Heberle, J.; Dencher, N. A., Surface-bound optical probes monitor proton translocation and surface-potential changes during the bacteriorhodopsin photocycle. *Proc. Natl. Acad. Sci. U.S.A.* **1992,** *89* (13), 5996-6000.

6. Drachev, L. A.; Kaulen, A. D.; Skulachev, V. P., Correlation of photochemical cycle, H+ release and uptake, and electric events in bacteriorhodopsin. *FEBS Lett.* **1984,** *178* (2), 331-335.

7. Zhang, C.; Knyazev, D. G.; Vereshaga, Y. A.; Ippoliti, E.; Nguyen, T. H.; Carloni, P.; Pohl, P., Water at hydrophobic interfaces delays proton surface-to-bulk transfer and provides a pathway for lateral proton diffusion. *Proc. Natl. Acad. Sci. U.S.A.* **2012,** *109* (25), 9744-9749.

8. Wolf, Maarten G.; Grubmüller, H.; Groenhof, G., Anomalous surface diffusion of protons on lipid membranes. *Biophys. J.* **2014,** *107* (1), 76-87.

9. Yamashita, T.; Voth, G. A., Properties of hydrated excess protons near phospholipid bilayers. *J. Phys. Chem. B* **2010,** *114* (1), 592-603.

10. Re, S.; Nishima, W.; Tahara, T.; Sugita, Y., Mosaic of water orientation structures at a neutral zwitterionic lipid/water interface revealed by molecular dynamics simulations. *J. Phys. Chem. Lett.* **2014,** *5* (24), 4343-4348.

11. Toppozini, L.; Roosen-Runge, F.; I. Bewley, R.; M. Dalgliesh, R.; Perring, T.; Seydel, T.; Glyde, H. R.; Garcia Sakai, V.; Rheinstadter, M. C., Anomalous and anisotropic nanoscale diffusion of hydration water molecules in fluid lipid membranes. *Soft Matter* **2015,** *11* (42), 8354-8371.

12. Gutman, M.; Nachliel, E., The dynamics of proton exchange between bulk and surface groups. *Biochim. Biophys. Acta, Bioenerg.* **1995,** *1231* (2), 123-138.

13. Gennis, R. B., Proton dynamics at the membrane surface. *Biophys. J.* **2016,** *110* (9), 1909-1911.

14. Stuchebrukhov, A. A.; Variyam, A. R.; Amdursky, N., Using proton geminate recombination as a probe of proton migration on biological membranes. *J. Phys. Chem. B* **2022,** *126* (32), 6026-6038.

15. Medvedev, E. S.; Stuchebrukhov, A. A., Mechanism of long-range proton translocation along biological membranes. *FEBS lett.* **2013,** *587* (4), 345-349.

16. Medvedev, E. S.; Stuchebrukhov, A. A., Proton diffusion along biological membranes. *J. Phys.: Condens. Matter* **2011,** *23* (23), 234103.

17. Medvedev, E. S.; Stuchebrukhov, A. A., Kinetics of proton diffusion in the regions of fast and slow exchange between the membrane surface and bulk solution. *J. Math. Biol.* **2005,** *52*, 209-234.

18. Georgievskii, Y.; Medvedev, E. S.; Stuchebrukhov, A. A., Proton transport via coupled surface and bulk diffusion. *J. Chem. Phys.* **2002,** *116* (4), 1692-1699.

19. Georgievskii, Y.; Medvedev, E. S.; Stuchebrukhov, A. A., Proton transport via the membrane surface. *Biophys. J.* **2002,** *82* (6), 2833-46.

20. Springer, A.; Hagen, V.; Cherepanov, D. A.; Antonenko, Y. N.; Pohl, P., Protons migrate along interfacial water without significant contributions from jumps between ionizable groups on the membrane surface. *Proc. Natl. Acad. Sci. U.S.A.* **2011,** *108* (35), 14461-14466.

21. Sandén, T.; Salomonsson, L.; Brzezinski, P.; Widengren, J., Surface-coupled proton exchange of a membrane-bound proton acceptor. *Proc. Natl. Acad. Sci. U.S.A.* **2010,** *107* (9), 4129-4134.

22. Brändén, M.; Sandén, T.; Brzezinski, P.; Widengren, J., Localized proton microcircuits at the biological membrane–water interface. *Proc. Natl. Acad. Sci. U.S.A.* **2006,** *103* (52), 19766-19770.

23. Serowy, S.; Saparov, S. M.; Antonenko, Y. N.; Kozlovsky, W.; Hagen, V.; Pohl, P., Structural proton diffusion along lipid bilayers. *Biophys. J.* **2003,** *84* (2), 1031-1037.

24. Amdursky, N.; Lin, Y., Tracking subtle membrane disruptions with a tethered photoacid. *ChemPhotoChem* **2020,** *4* (8), 592-600.

25. Amdursky, N.; Lin, Y.; Aho, N.; Groenhof, G., Exploring fast proton transfer events associated with lateral proton diffusion on the surface of membranes. *Proc. Natl. Acad. Sci. U.S.A.* **2019,** *116* (7), 2443-2451.

26. Mueller, P. R., D. O.; Ti Tien, H.; Wescott, W. C., Reconstitution of cell membrane structure in vitro and its transformation into an excitable system. *Nature* **1962,** *194*, 979-980.

27. Benz, R.; Frohlich, O.; Lauger, P.; Montal, M., Electrical capacity of black lipid films and of lipid bilayers made from monolayers. *Biochim. Biophys. Acta* **1975,** *394* (3), 323-334.

28. Miyamoto, V. K.; Thompson, T. E., Some electrical properties of lipid bilayer membranes. *J. Colloid Interface Sci.* **1967,** *25* (1), 16.

29. Tamm, L. K.; McConnell, H. M., Supported phospholipid-bilayers. *Biophys. J.* **1985,** *47* (1), 105-113.

30. Liu, H. Y.; Chen, W. L.; Ober, C. K.; Daniel, S., Biologically complex planar cell plasma membranes supported on polyelectrolyte cushions enhance transmembrane protein mobility and retain native orientation. *Langmuir* **2018,** *34* (3), 1061-1072.

31. Richards, M. J.; Hsia, C. Y.; Singh, R. R.; Haider, H.; Kumpf, J.; Kawate, T.; Daniel, S., Membrane protein mobility and orientation preserved in supported bilayers created directly from cell plasma membrane blebs. *Langmuir* **2016,** *32* (12), 2963-2974.

32. Tanaka, M.; Sackmann, E., Polymer-supported membranes as models of the cell surface. *Nature* **2005,** *437* (7059), 656-663.

33. Lubrano, C.; Matrone, G. M.; Iaconis, G.; Santoro, F., New Frontiers for Selective Biosensing with Biomembrane-Based Organic Transistors. *ACS Nano* **2020,** *14* (10), 12271-12280.

34. Su, H.; Liu, H. Y.; Pappa, A. M.; Hidalgo, T. C.; Cavassin, P.; Inal, S.; Owens, R. M.; Daniel, S., Facile generation of biomimetic-supported lipid bilayers on conducting polymer surfaces for membrane biosensing. *ACS Appl. Mater. Interfaces* **2019,** *11* (47), 43799-43810.

35. Bally, M.; Bailey, K.; Sugihara, K.; Grieshaber, D.; Voros, J.; Stadler, B., Liposome and lipid bilayer arrays towards biosensing applications. *Small* **2010,** *6* (22), 2481-2497.

36. Wiegand, G.; Arribas-Layton, N.; Hillebrandt, H.; Sackmann, E.; Wagner, P., Electrical properties of supported lipid bilayer membranes. *J. Phys. Chem. B* **2002,** *106* (16), 4245-4254.

37. Lu, Z. X.; van Niekerk, D.; Savva, A.; Kallitsis, K.; Thiburce, Q.; Salleo, A.; Pappa, A. M.; Owens, R. M., Understanding electrochemical properties of supported lipid bilayers interfaced with organic electronic devices. *J. Mater. Chem. C* **2022,** *10* (20), 8050-8060.

38. Hillebrandt, H.; Wiegand, G.; Tanaka, M.; Sackmann, E., High electric resistance polymer/lipid composite films on indium-tin-oxide electrodes. *Langmuir* **1999,** *15* (24), 8451-8459.

39. Steinem, C.; Janshoff, A.; Galla, H. J.; Sieber, M., Impedance analysis of ion transport through gramicidin channels incorporated in solid supported lipid bilayers. *Bioelectrochem. Bioenerg.* **1997,** *42* (2), 213-220.

40. Bert Sakmann, E. N., *Single-channel recording*. Plenum Press: New York: 1985.

41. Riquelme, G.; Lopez, E.; Garcia-Segura, L. M.; Ferragut, J. A.; Gonzalez-Ros, J. M., Giant liposomes: a model system in which to obtain patch-clamp recordings of ionic channels. *Biochemistry* **1990,** *29* (51), 11215-11222.

42. Delcour, A.; Martinac, B.; Adler, J.; Kung, C., Modified reconstitution method used in patch-clamp studies of Escherichia coli ion channels. *Biophys. J.* **1989,** *56* (3), 631-636.

43. Cremer, P. S.; Boxer, S. G., Formation and spreading of lipid bilayers on planar glass supports. *J. Phys. Chem. B* **1999,** *103* (13), 2554-2559.

44. Mennicke, U.; Salditt, T., Preparation of solid-supported lipid bilayers by spin-coating. *Langmuir* **2002,** *18* (21), 8172-8177.

45. Richter, R. P.; Berat, R.; Brisson, A. R., Formation of solid-supported lipid bilayers: An integrated view. *Langmuir* **2006,** *22* (8), 3497-3505.

46. Amit, M.; Roy, S.; Deng, Y. X.; Josberger, E.; Rolandi, M.; Ashkenasy, N., Measuring proton currents of bioinspired materials with metallic contacts. *ACS Appl. Mater. Interfaces* **2018,** *10* (2), 1933-1938.

47. Deng, Y. X.; Josberger, E.; Jin, J. H.; Rousdari, A. F.; Helms, B. A.; Zhong, C.; Anantram, M. P.; Rolandi, M., H+-type and OH--type biological protonic semiconductors and complementary devices. *Sci. Rep.* **2013,** *3*, 2481.

48. Josberger, E. E.; Hassanzadeh, P.; Deng, Y. X.; Sohn, J.; Rego, M. J.; Amemiya, C. T.; Rolandi, M., Proton conductivity in ampullae of Lorenzini jelly. *Sci. Adv.* **2016,** *2* (5), e1600112.

49. Selberg, J.; Jia, M. P.; Rolandi, M., Proton conductivity of glycosaminoglycans. *PLoS One* **2019,** *14* (3), e0202713.

50. Zhong, C.; Deng, Y. X.; Roudsari, A. F.; Kapetanovic, A.; Anantram, M. P.; Rolandi, M., A polysaccharide bioprotonic field-effect transistor. *Nat. Commun.* **2011,** *2*, 276.

51. Binder, H., Water near lipid membranes as seen by infrared spectroscopy. *Eur. Biophys. J.* **2007,** *36* (4-5), 265-279.

52. Binder, H., The molecular architecture of lipid membranes - New insights from hydration-tuning infrared linear dichroism spectroscopy. *Appl. Spectrosc. Rev.* **2003,** *38* (1), 15-69.

53. Binder, H.; Anikin, A.; Kohlstrunk, B.; Klose, G., Hydration-induced gel states of the dienic lipid 1,2-bis(2,4-octadecadienoyl)-sn-glycero-3-phosphorylcholine and their characterization using infrared spectroscopy. *J. Phys. Chem. B* **1997,** *101* (33), 6618-6628.

54. Binder, H.; Pohle, W., Structural aspects of lyotropic solvation-induced transitions in phosphatidylcholine and phosphatidylethanolamine assemblies revealed by infrared spectroscopy. *J. Phys. Chem. B* **2000,** *104* (50), 12039-12048.

55. Nilsson, A.; Holmgren, A.; Lindblom, G., Fourier-transform infrared-spectroscopy study of dioleoylphosphatidylcholine and monooleoylglycerol in lamellar and cubic liquid-crystals. *Biochem.* **1991,** *30* (8), 2126-2133.

56. Kint, S.; Wermer, P. H.; Scherer, J. R., Raman spectra of hydrated phospholipid bilayers .2. Water and head group interactions. *J. Phys. Chem.* **1992,** *96* (1), 446-452.

57. Grdadolnik, J.; Kidric, J.; Hadzi, D., Hydration of phosphatidylcholine reverse micelles and multilayers - an infrared spectroscopy study. *Chem. Phys. Lipids* **1991,** *59* (1), 57-68.

58. Nandi, R.; Agam, Y.; Amdursky, N., A protein-based free-standing proton-conducting transparent elastomer for large-scale sensing applications. *Adv. Mater.* **2021,** *33* (32), 2101208.

59. Amdursky, N.; Wang, X. H.; Meredith, P.; Bradley, D. D. C.; Stevens, M. M., Long-range proton conduction across free-standing serum albumin mats. *Adv. Mater.* **2016,** *28* (14), 2692-2698.

60. Yang, Z. Y.; Sarkar, A. K.; Amdursky, N., Glycoproteins as a platform for making proton-conductive free-standing biopolymers. *Biomacromolecules* **2023,** *24* (3), 1111-1120.

61. Deng, Y. X.; Helms, B. A.; Rolandi, M., Synthesis of pyridine chitosan and its protonic conductivity. *J. Polym. Sci., Part A: Polym. Chem.* **2015,** *53* (2), 211-214.

62. Ma, C.; Dong, J. J.; Viviani, M.; Tulini, I.; Pontillo, N.; Maity, S.; Zhou, Y.; Roos, W. H.; Liu, K.; Herrmann, A.; Portale, G., De novo rational design of a freestanding, supercharged polypeptide, proton-conducting membrane. *Sci. Adv.* **2020,** *6* (29), eabc0810.

63. Pena-Francesch, A.; Jung, H.; Hickner, M. A.; Tyagi, M.; Allen, B. D.; Demirel, M. C., Programmable proton conduction in stretchable and self-healing proteins. *Chem. Mater.* **2018,** *30* (3), 898-905.

64. Ordinario, D. D.; Phan, L.; Walkup, W. G.; Jocson, J. M.; Karshalev, E.; Husken, N.; Gorodetsky, A. A., Bulk protonic conductivity in a cephalopod structural protein. *Nat. Chem.* **2014,** *6* (7), 597-603.

65. Lerner Yardeni, J.; Amit, M.; Ashkenasy, G.; Ashkenasy, N., Sequence dependent proton conduction in self-assembled peptide nanostructures. *Nanoscale* **2016,** *8* (4), 2358-2366.

66. Silberbush, O.; Amit, M.; Roy, S.; Ashkenasy, N., Significant Enhancement of Proton Transport in Bioinspired Peptide Fibrils by Single Acidic or Basic Amino Acid Mutation. *Adv. Funct. Mater.* **2017,** *27* (8), 1604624.

67. Agam, Y.; Nandi, R.; Bulava, T.; Amdursky, N., The role of the protein-water interface in dictating proton conduction across protein-based biopolymers. *Mater. Adv.* **2021,** *2* (5), 1739-1746.

68. Mondal, S.; Agam, Y.; Nandi, R.; Amdursky, N., Exploring long-range proton conduction, the conduction mechanism and inner hydration state of protein biopolymers. *Chem. Sci.* **2020,** *11* (13), 3547-3556.

69. Agmon, N., The Grotthuss mechanism. *Chem. Phys. Lett.* **1995,** *244* (5-6), 456-462.

70. Knight, C.; Voth, G. A., The Curious Case of the Hydrated Proton. *Acc. Chem. Res.* **2012,** *45* (1), 101-109.

71. Steiner, T., The hydrogen bond in the solid state. *Angew. Chem. Int. Ed.* **2002,** *41* (1), 48-76.

72. Agmon, N.; Gutman, M., Bioenergetics: Proton fronts on membranes. *Nat. Chem.* **2011,** *3* (11), 840-842.

73. Freier, E.; Wolf, S.; Gerwert, K., Proton transfer via a transient linear water-molecule chain in a membrane protein. *Proc. Natl. Acad. Sci. U.S.A.* **2011,** *108* (28), 11435-11439.

74. Cui, Q.; Karplus, M., Is a "proton wire" concerted or stepwise? A model study of proton transfer in carbonic anhydrase. *J. Phys. Chem. B* **2003,** *107* (4), 1071-1078.

75. Tarnapolsky, A.; Freger, V., Modeling QCM-D response to deposition and attachment of microparticles and living cells. *Anal. Chem.* **2018,** *90* (23), 13960-13968.

76. Sauerbrey, G., Use of quartz crystals for weighing thin films and microweighing. *Z. Physik* **1959,** *155*, 206-222.